Available online at www.sciencedirect.com
ScienceDirect
Trans. Nonferrous Met. Soc. China 30(2020) 288−302
Transactions of Nonferrous Metals Society of China
www.tnmsc.cn

Effects of yttrium addition and aging on mechanical properties of AA2024 fabricated through multi-step stir casting

CH. S. VIDYASAGAR[1], D. B. KARUNAKAR[2]

1. Metallurgical and Materials Engineering Department, Indian Institute of Technology Roorkee - 247667, India;
2. Mechanical and Industrial Engineering Department, Indian Institute of Technology Roorkee - 247667, India

Received 14 May 2019; accepted 21 November 2019

Abstract: The effects of yttrium and artificial aging on AA2024 alloy were investigated. The developed samples were further subjected to artificial aging at 190 °C for 1−10 h with an interval of 1 h. The metallurgical characterization was done by scanning electron microscope and X-ray diffraction. The mechanical characterization like hardness and tensile strength of the samples was done using computerized Vickers hardness testing machine and universal testing machine. The microstructures revealed that addition of yttrium refined the α(Al) matrix and led to the formation of Al−Cu−Y intermetallic in the shape of Chinese script which strengthened the samples. Compared to the base metal, samples with yttrium addition showed better mechanical properties. The sample reinforced with 0.3 wt.% yttrium showed the highest mechanical properties with the hardness of 66 HV, UTS of 223 MPa, YS of 180 MPa, and elongation of 20.9%. The artificially aged samples showed that the peak hardening of all the samples took place within 5 h of aging at 190 °C with Al_2Cu precipitation. Aging changed the intermetallic from Chinese script to the fibrous form. The optimum amount of yttrium addition to AA2024 was found to be 0.3 wt.%.

Key words: yttrium; artificial aging; mechanical properties; multi-step stir casting; precipitation; microstructure characterization

1 Introduction

Due to the rapid change in technology from time to time, there is an immense pressure on material science engineers to develop stronger, lighter and cheaper materials, which can fulfill the recent needs. In the process of meeting this demand, a unique method has been adopted, that is, the materials which have currently been used in certain applications are further developed by alloying with known metals, methods of grain modifications, various heat treatments, secondary processing, etc. However, the development of materials through alloying has reached its limit and establishing new alloy systems is a time taking process [1]. Therefore, new trends and innovations must emerge in developing new materials with improved tailored properties at decreasing cost and improved efficiency. Three decades ago, completely new generation materials with properties that could be tailored to the requirements of a certain application appeared. Addition of trace elements provided scope to modify the precipitation kinetics in aluminium alloys. Among the metals, aluminium alloys were continuously given preference in research due to their high specific strength and low density. Further, aluminium based alloys and metal matrix composites (AMMCs) took lead in various disciplines, as they remain as potential candidates for making advanced structural and engineering components with greater efficiency [2−6].

Research around the world in the area of aluminium alloys proved beyond doubt the efficiency of aluminium matrix composites over base alloys not only in the laboratory but also at

Corresponding author: D. B. KARUNAKAR; E-mail: bennyfme@iitr.ac.in
DOI: 10.1016/S1003-6326(20)65213-X

industrial scale. However, the efficiency of the properties of these depends on the factors like, (1) distribution of precipitates in the matrix; (2) shape, size and amount of precipitation; (3) type of intermetallics formed between the matrix and the element added [7−9].

The above factors are solely dependent on the processing method. Among various processing methods used for developing AMMCs, liquid metallurgy is an ancient classic method and widely preferred due to its ease of operation. On the other hand, other fabrication methods are more effective concerning the improvements in microstructure and properties attained. However, the ease of operation decreased wastage of material through reuse, cost economics, etc., which has established the liquid metallurgy as a successful, competitive and go-to method for fabricating aluminum matrix composites, especially those of bigger size [10].

Over the years, a huge amount of research and development has gone into aluminium matrix composites with every possible aluminium alloy as matrix, i.e., 2xxx to 7xxx series with different types of reinforcing elements. However, the choice of matrix, selection of trace element (type, size and amount) and processing method depend on the application of the product developed. Among various aluminium alloys, Al−Cu and Al−Zn alloys are extensively used as matrix materials to develop engineering components, which can resist a certain amount of mechanical degradation to a maximum limit [11,12]. Based on the available literature on aluminium alloys, it can be observed that the Al−Cu alloy has been extensively studied concerning precipitation kinetics and aging mechanism. This alloy has been the focus of interest to the researchers with respect to understanding the strengthening mechanisms, precipitation, and its corresponding properties. However, it is well known that the addition of reinforcement of more than 15 wt.% tremendously increases the overall cost of the composite.

A viable solution to the present problem could be found when the properties of the materials are improved with very little addition of an appropriate element. Research reports on rare earth elements as minor alloying elements showed positive effects on the mechanical properties of various aluminium alloys. It was reported that minor addition of Ce improved the thermal stability of the Ω phase and thus, increased the service temperature of Al−Cu−Mg−Ag alloy [13]. Recently, ZOU et al [14] studied the effect of Yb on the grain refinement of ADC12 aluminium alloy and reported that there was an obvious grain refinement. SHI et al [15] reported that the addition of Gd had an excellent refining effect on primary A365 α(Al) grains and secondary Si phase was modified by casting. With additional T6 treatment, the needle-like Si phases were modified to fine particles and uniformly distributed in the matrix which improved the mechanical properties, especially for the alloy with 0.2 wt.% Gd addition. WANG et al [16] reported that addition of 0.5 wt.% Sb to Al−20Mg2Si−4Cu alloy was effective in refining the microstructure by modifying primary Mg_2Si from coarse dendrite into smaller polyhedral shape with average size less than 20 mm. The authors also stated that the tensile properties of the Sb modified alloy were improved compared to the base alloy at both room temperature and 150 °C. LI et al [17] reported that with addition of 0.5% Er to Al−20Si alloy, primary Si was significantly refined from coarse polygonal, platelet-like and star-like shape to fine blocky shape, and eutectic Si structure was modified from coarse needles to the fine fibrous structure along with an increase in the mechanical properties. However, the primary and eutectic Si phases became coarser when the level of rare earth Er addition increased beyond 0.5%. Along with these, several other RE elements were used in aluminium alloys such as Sm [18], Ce [19], Eu [20], Sc [21], Nd [22] and Y [23], to improve their properties. Some researchers have introduced double RE elements together, such as La+Ce [24], Pr+Ce [25] and La+Yb [26], for grain modification and improvement in mechanical properties of various aluminium alloys.

From the literature, it can be observed that most of the RE additions were done to modify Al−Si alloys. Moreover, very less number of investigations on the modification of Al−Cu alloys can be found such as the addition of Ce [13], Yb [27], Nd [28], Sc [29], Er [30] and Y [31]. However, very less work has been focused and limited information is available on the addition of yttrium to Al−Cu alloys, especially, AA2024.

Therefore, the present study is focused on developing the Al−Cu matrix by adding varying amounts of micro yttrium ranging from 0.1 to

0.5 wt.% through multi-step stir casting. The effects of yttrium addition and multi-step stirring on the microstructure and mechanical properties are evaluated.

2 Experimental

Cylindrical bars of AA2024 (99% in purity) and yttrium powder (99.6% in purity), were procured from Alfa Aesar, United States. The as-received AA2024 cylindrical bars had composition given in Table 1.

Table 1 Chemical composition of as-received AA2024 cylindrical bar (wt.%)

Si	Fe	Cu	Mn	
0.50	0.50	3.80−4.90	0.30−0.90	
Mg	Cr	Zn	V	Al
1.20−1.80	0.10	0.25	0.005	Bal.

During melting of AA2024, some material loss may happen due to dross formation or burnout of alloying elements. In the present work, the loss of alloying elements during melting is considered negligible. However, after solidification, it is assumed that the composition of alloying elements falls in the range given in Table 1. The samples were stir cast in multiple steps by the following procedure. First, 200 g of AA2024 pieces were melted in a furnace at 800 °C. Once the pieces were melted and liquified, the pre-heated yttrium powder folded in aluminium foil was introduced into the melt at every step of stirring. Since the melting temperature of yttrium is 1526 °C, burning of yttrium during stirring may not have happened. The stirring speed was gradually increased and the temperature was increased to 900 °C to compensate for the cooling effect developed during stirring. After 10 min of stirring at 100 r/min, the liquid melt was allowed to settle down and again stirring was introduced. This procedure was continued until the melt became semi-solid. Then, the temperature was again raised beyond the melting temperature and the molten charge was poured into a steel die with dimensions of 15 mm × 30 mm × 250 mm and allowed to cool at room temperature. The stir cast samples with varying amounts of yttrium addition are shown in Fig. 1.

The entire process was carried out at normal atmosphere and pressure (no special atmosphere was used). After the melt was solidified and cooled down to room temperature, the samples were removed from the die. Then, the samples were cut into pieces for further mechanical and metallurgical investigations. After the samples were cut for characterization, the remains of each sample were stored in a refrigerator to avoid any natural aging. Further, all the samples were subjected to artificial aging. Initially, all the samples were solutionized by heating them to a solid solution temperature of 500 °C and quenched to room temperature by water. Next, each solutionized sample was cut into ten pieces and then placed in a furnace until the furnace reached a temperature of 190 °C. Once all the pieces of all the samples in the furnace reached 190 °C, time was noted. One hour after the noted time, one piece from each sample was taken out for characterization. In order to evaluate the effect of heating time on the hardening of the samples, corresponding pieces from each sample were taken out with an interval of 1 h up to 10 h.

Fig. 1 Stir cast samples with varying amounts of yttrium addition

3 Results

3.1 Density

The samples developed through the above said stir casting process were cut into small pieces of equal size for measurement of experimental density. The theoretical and experimental densities of the samples were calculated by rule of mixtures and Archimedes principle, according to ASTM B962-08 standard. The relative density was calculated using the theoretical and experimental densities and its variation with respect to the increase in yttrium addition is shown in Fig. 2.

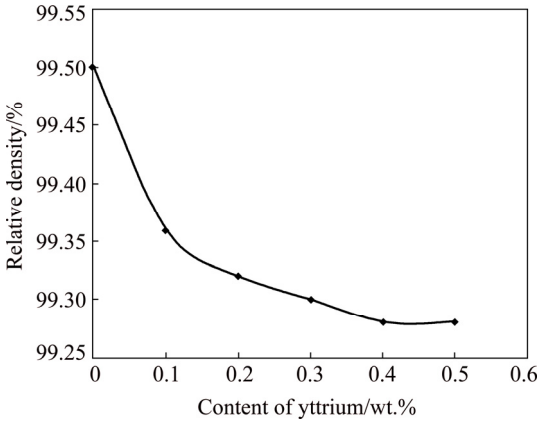

Fig. 2 Variation of relative density of multi-step stir cast samples with varying amounts of yttrium addition

Yttrium addition to AA2024 matrix has decreased the relative density of the samples compared to the as-received AA2024 ingots. From Fig. 1, it can be observed that the relative density of the samples decreases steeply up to 0.3 wt.% of yttrium addition. Upon further increase in yttrium addition, the decrease in relative density is not significant.

Figure 3 shows the XRD patterns of the samples with various amounts of yttrium addition after stir casting. From Fig. 3, it can be seen that phases like Al_3Y, Al_6Cu_6Y and Al_2Cu are present in the samples and their amounts increase with yttrium addition. Also, it is observed that the peak ratio of Al_3Y in the sample with 0.4 wt.% yttrium is higher than that in the sample with 0.5 wt.% yttrium. This difference in the peak ratios depends on many factors, for instance, preferred growth in a particular plane, experimental conditions, and instrument error.

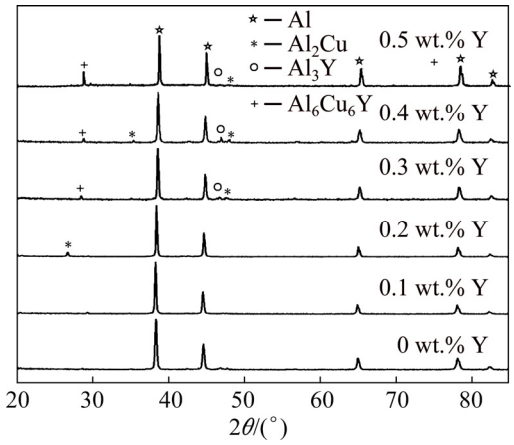

Fig. 3 XRD patterns of samples with varying amounts of yttrium addition

3.2 Microstructure

The samples were cut into small pieces, ground and then polished on silicon carbide emery papers. The polished samples were further polished on a mechanical rotating coarse cloth disc with fine Al_2O_3 powder particles until the visible scratches were removed and a mirror-like finish was obtained. The samples were etched for 30−40 s with modified Keller's reagent which was prepared by mixing 10 mL HNO_3, 1.5 mL HCl, 1 mL HF (48 wt.%), and distilled water. Then, the samples were thoroughly examined by field emission scanning electron microscope (FE-SEM). Figure 4 shows the FE-SEM microstructures of the stir cast samples with varying amounts of yttrium addition.

From the microstructures in Fig. 4, it can be observed that the grain refinement of the aluminium matrix takes place gradually with the increase in the amount of yttrium addition compared to that of the unreinforced AA2024. The formation of the intermetallic compound (Al−Cu−Y) in the matrix leads to the formation of grains. As the yttrium content is increased up to 0.3 wt.%, there is a positive response to grain refinement. Gradually, the grains start to form, leading to grain refinement. Upon further increase in yttrium content, the grain refinement and grain size reduction are not clear. Figure 5 shows the variation of the average grain size of the samples with yttrium addition.

From Fig. 5, it can be observed that the addition of yttrium remarkably reduces the grain size up to 0.3 wt.% and the grains start to coarsen with further increase in yttrium addition. The increase in the average grain size beyond 0.3 wt.% yttrium addition is not as significant as the grain size reduction up to 0.3 wt.% Y addition. The average grain sizes of the samples were calculated using Image J software. The calculated average grain sizes of the samples with 0, 0.1, 0.2, 0.3, 0.4 and 0.5 wt.% Y are 532, 467, 396, 323, 366 and 388 μm, respectively.

For further investigation, the samples were examined through FE-SEM in back-scatter mode at higher magnification to observe the intermetallic phase formation and its transformation in the matrix. The back-scattered FE-SEM images are shown in Fig. 6. The microstructures exhibit two distinct types of secondary phases in the α(Al) matrix, which play an important role in the variation in the strength of the samples. From Fig. 6, it is evident

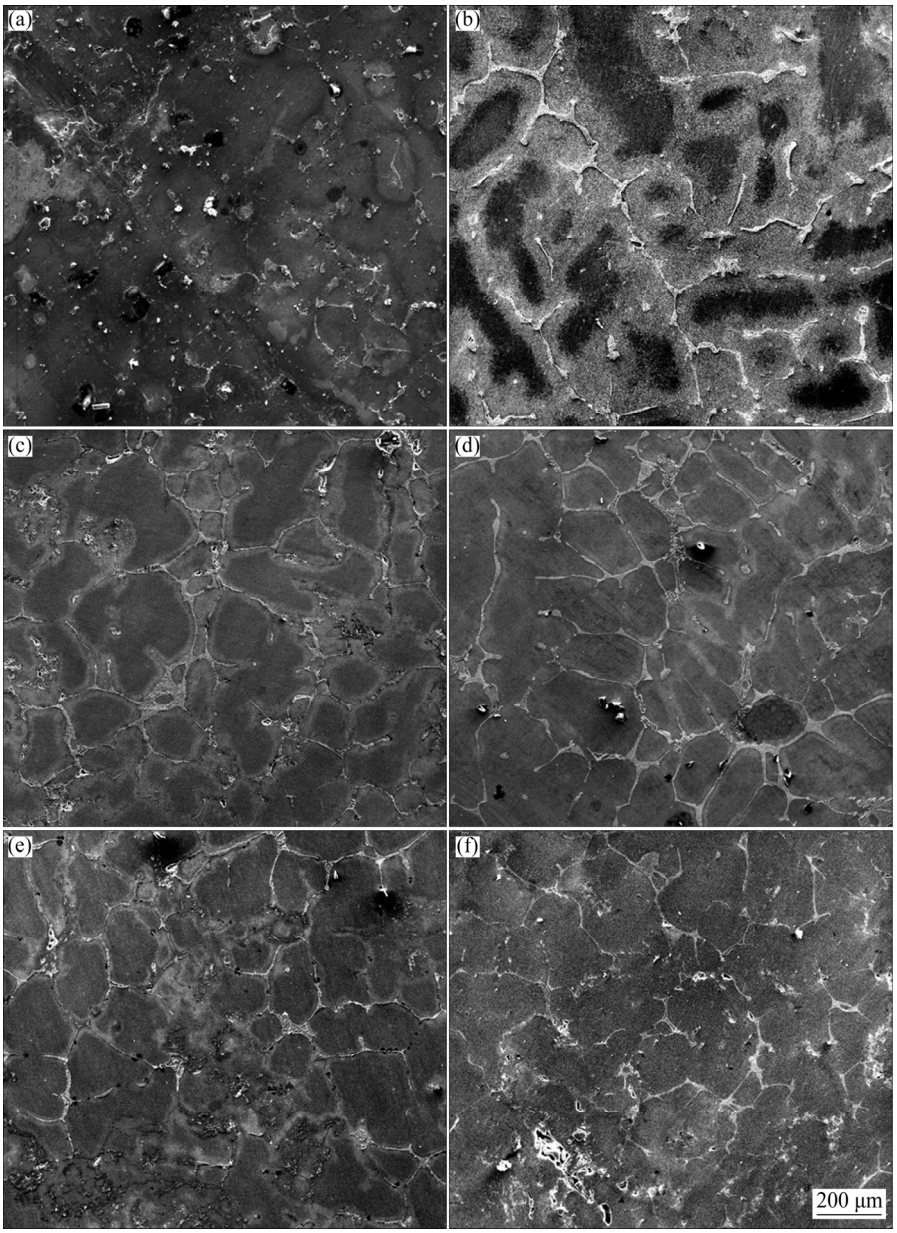

Fig. 4 FE-SEM images of stir cast samples reinforced with different amounts of yttrium: (a) 0 wt.%; (b) 0.1 wt.%; (c) 0.2 wt.%; (d) 0.3 wt.%; (e) 0.4 wt.%; (f) 0.5 wt.%

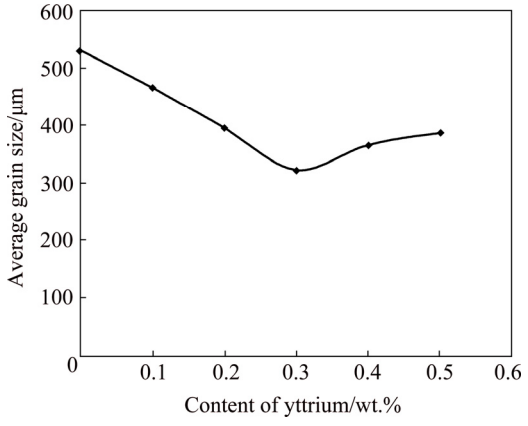

Fig. 5 Variation of average grain size of samples with yttrium addition

that the addition of 0.1 wt.% yttrium leads to the formation of a Chinese script phase in the matrix. EDAX analysis shows that the Chinese script phase has the composition rich in Al, Cu and Y. Apart from the Chinese script phase, another phase comprising Al and Cu as major elements can also be seen in the matrix. As the yttrium addition increases up to 0.3 wt.%, the Chinese script phase becomes finer. Upon further increase in yttrium addition, the Chinese script phase coarsens (encircled in white) along with the Al−Cu phase, which is encircled in red.

The SE-SEM image showing the Al−Y−Cu

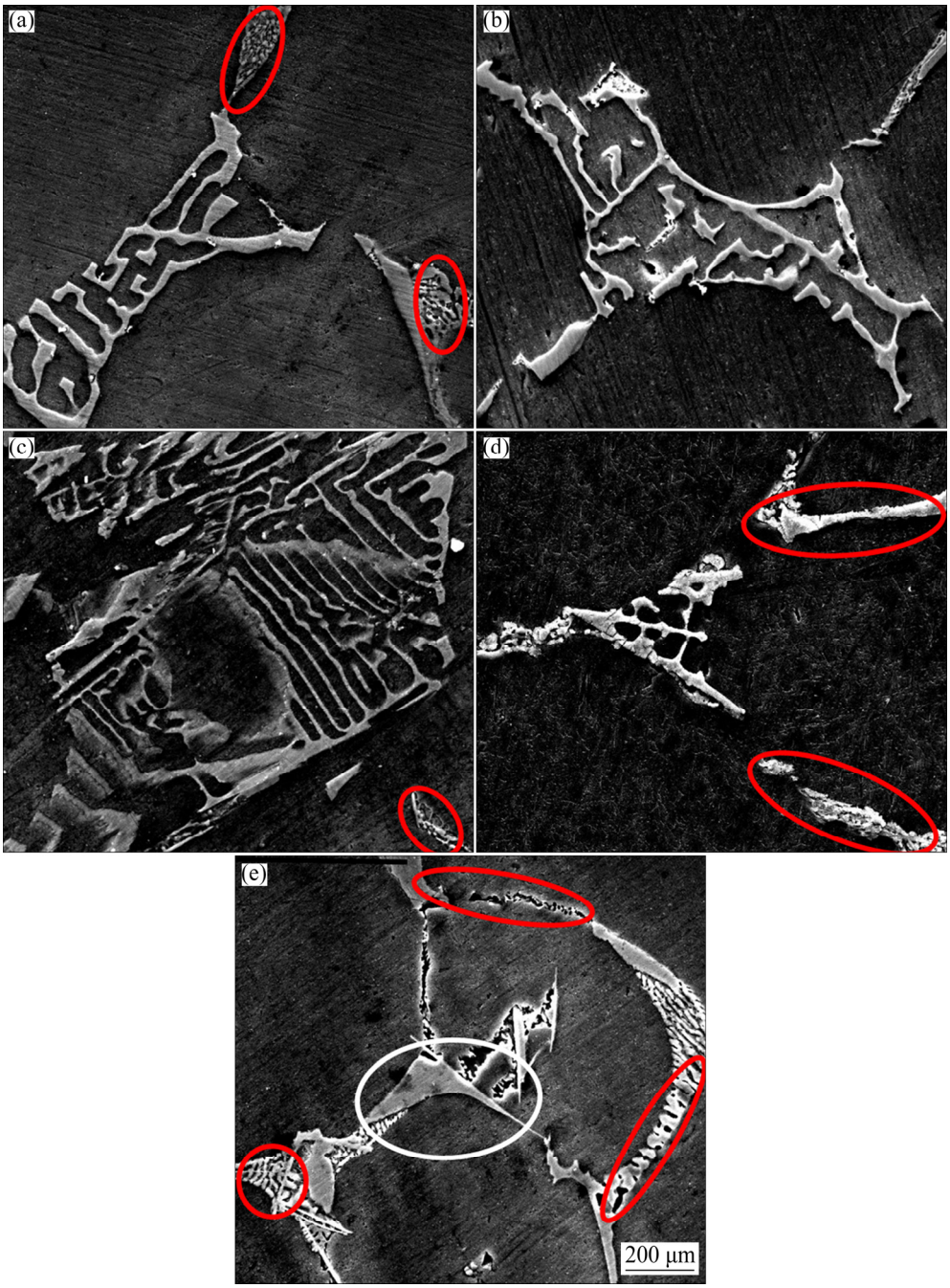

Fig. 6 FE-SEM back-scattered images at higher magnification showing secondary phases and intermetallic transformation in stir cast samples added with different amounts of yttrium: (a) 0.1 wt.%; (b) 0.2 wt.%; (c) 0.3 wt.%; (d) 0.4 wt.%; (e) 0.5 wt.%

intermetallic formation of the sample with 0.3 wt.% yttrium addition is shown in Fig. 7. Further, EDAX analysis was carried out to quantify various elements present in the respective phases in the matrix and the elemental spectra of the selected points are shown in Figs. 7(c−f). The elemental spectra show the intensity of the elements present in the selected points of interest in the microstructure. Table 2 gives the approximate mass fraction of different elements at various selected points in the sample.

From Fig. 7(a), it can be observed that two distinct types of phases are present in the matrix. They constitute an intermetallic Al−Y−Cu phase resembling Chinese script shape, outlined in a white rectangle, and an Al−Cu phase encircled in red.

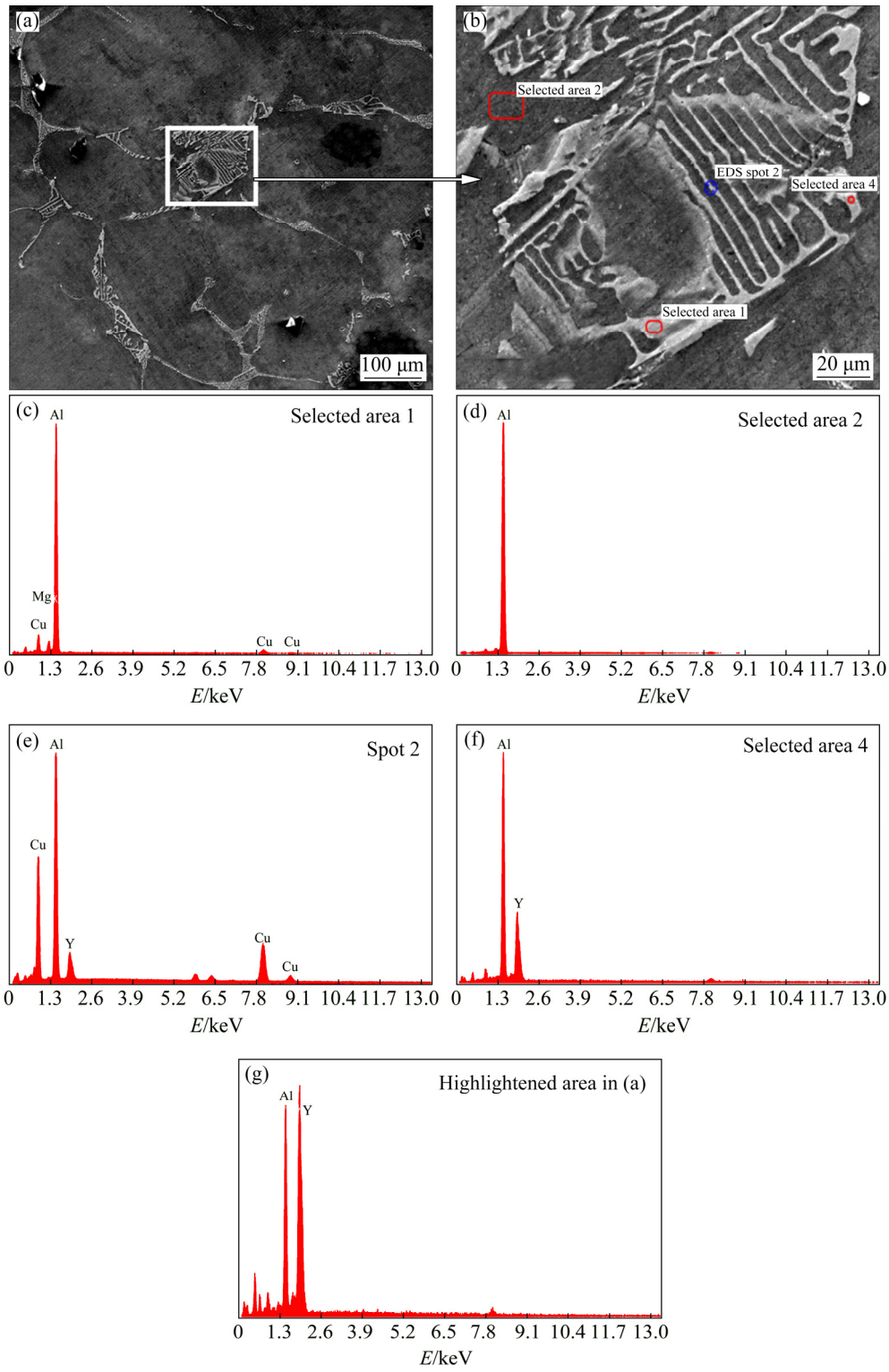

Fig. 7 FE-SEM images of stir cast sample with 0.3 wt.% yttrium addition (a, b) and EDAX elemental spectra (c−g)

Table 2 Approximate composition of elements in sample with 0.3 wt.% yttrium addition calculated by EDAX (wt.%)

Element	Selected area 1	Selected area 2	Spot 2	Selected area 4
Al	97.6	99.5	42.22	76.52
Y	0	0	12.4	50.28
Cu	12.4	0.5	45.38	0

Figure 7(b) shows the intermetallic Chinese script phase at a higher magnification showing the selected points for EDAX elemental graph analysis.

Small pieces of all the samples were artificially aged at 190 °C for 1−10 h with a time interval of 1 h. Before the artificial aging treatment, the sample pieces were solutionized at 500 °C and water quenched to room temperature. The FE-SEM images of the samples heat-treated for 5 h at 190 °C are shown in Fig. 8.

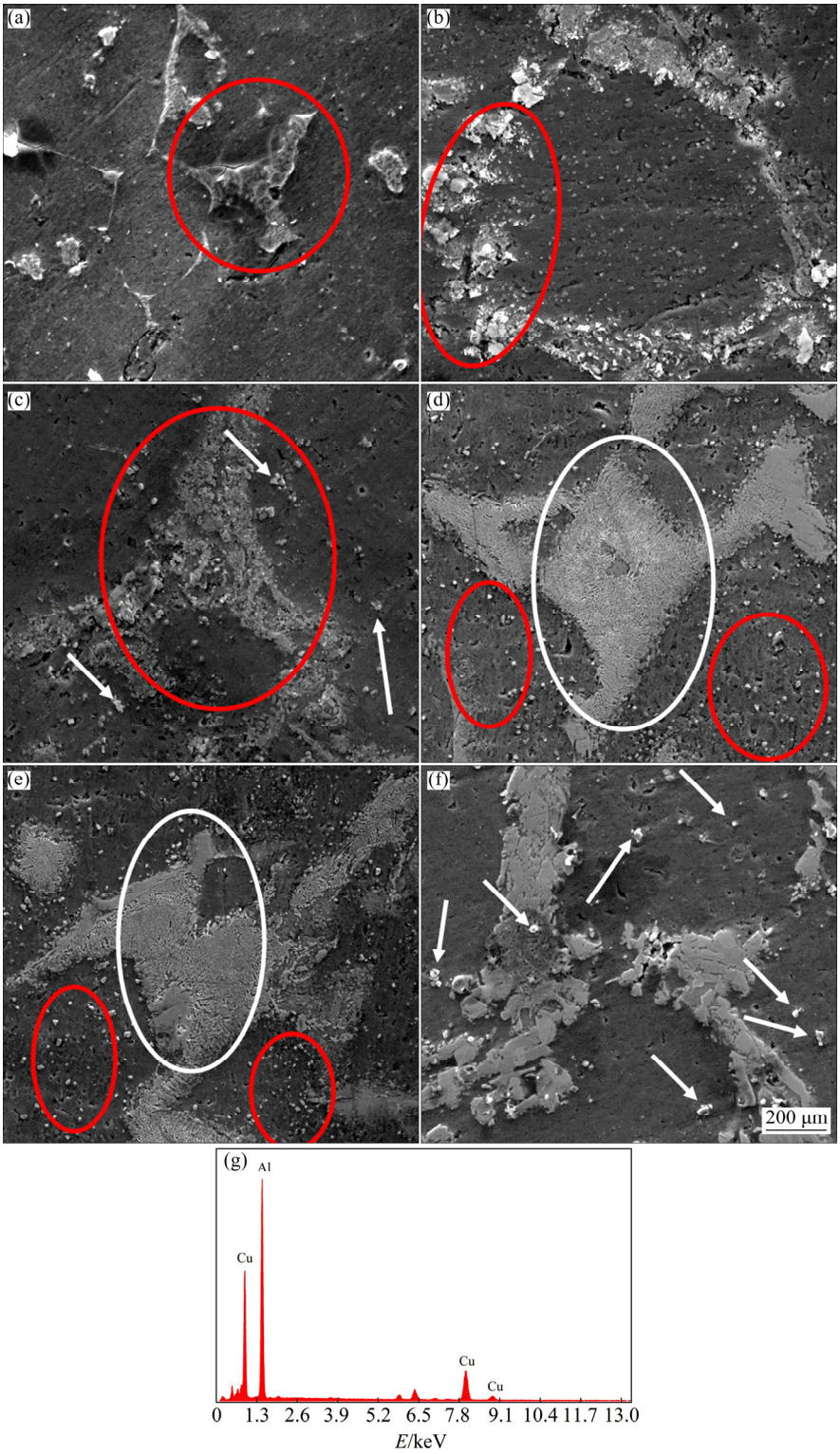

Fig. 8 FE-SEM back scattered images of stir cast samples heat-treated at 190 °C for 5 h (showing secondary phases) added with 0 wt.% (a), 0.1 wt.% (b), 0.2 wt.% (c), 0.3 wt.% (d), 0.4 wt.% (e) and 0.5 wt.% (f) Y, and EDX spectrum (g) of precipitates seen in (d)

From Fig. 8, two different kinds of phases can be observed, which are indicated with circles and arrows in the microstructures. Due to heat treatment, evidence of precipitation is seen in the microstructures of the samples. The fibrous phase present in Figs. 8(d, e) is an Al−Cu−Y intermetallic compound verified by the energy spectrum in Fig. 8(h) and the small white spots are Al_2Cu precipitates that occur due to heat treatment. As the addition of yttrium increases, the amounts of the fibrous intermetallic phase consisting of Al, Cu, Y and Al_2Cu precipitation also increase in the α(Al) matrix. Beyond 0.3 wt.% yttrium addition, both the fibrous intermetallic phase and Al_2Cu precipitation coarsen.

3.3 Mechanical properties

The mechanical properties like hardness, UTS, YS and elongation of the stir cast samples were tested. The effects of yttrium addition and the processing conditions on hardness of all the sintered samples were evaluated by measuring microhardness using a computerized Vickers hardness testing machine (Model: FIE VM 50 PC). All the specimens were mirror polished and observed under a microscope, which was coupled to the machine. A diamond pointer was placed on the sample and a load of 5 kg was applied for a dwell time of 10 s and then removed. The size of the indentation caused by the diamond pyramid pointer on the sample was inversely proportional to the hardness of the corresponding samples. Ten hardness measurements were taken randomly at several places for each sample for better accuracy and precession. The average values and standard deviations of the results were calculated and reported. The hardness was measured in the transverse direction, which was perpendicular to the applied load during sintering. The tensile test was performed to evaluate the effect of yttrium addition and processing methods on the tensile strength and elongation of all the samples. The tests were conducted on a universal testing machine (UTM) (Model: H 75 KS) at a strain rate of 0.003 s^{-1}. Three tensile specimens were cut from each sintered sample and the average values and standard deviations were reported. The tensile specimens were cut using a wire-cut electric discharge machine (EDM) according to ASTM E8 standards. The hardness variation of the samples with an increasing amount of yttrium addition is shown in Fig. 9. From Fig. 9, it can be observed that the hardness of the samples increases up to 0.3 wt.% yttrium addition and decreases thereafter. A clear trend of increase and decrease can be seen with yttrium addition, compared to unreinforced AA2024.

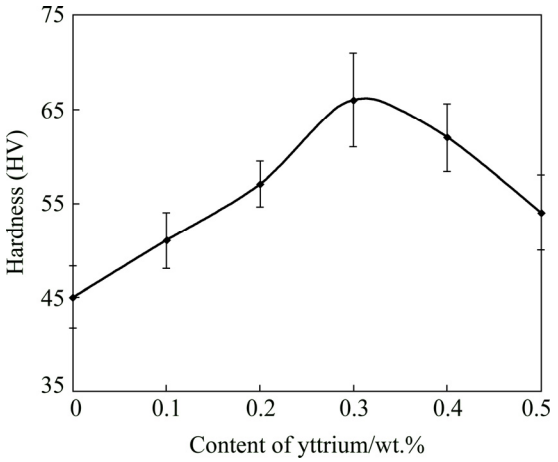

Fig. 9 Variation of hardness of stir cast samples with varying amounts of yttrium addition

The hardness of the samples heat-treated at 190 °C for various periods is shown in Fig. 10. The samples were taken out of the furnace at each time interval, water quenched and polished to determine the hardness.

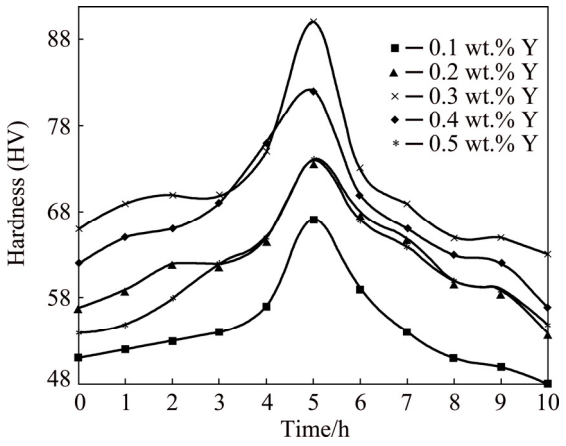

Fig. 10 Variation of hardness of stir cast samples heat-treated at 190 °C with respect to time and variation in yttrium addition

All the samples reach peak hardness within 5 h of heat treatment at 190 °C irrespective of the yttrium addition, as observed in Fig. 10. After 5 h of heat treatment, the samples got over-aged and before 5 h, they were under-aged. However, the

sample with 0.3 wt.% yttrium addition shows the highest hardness compared to the other samples at the peak aging time of 5 h.

Three tensile specimens were cut from each stir cast sample including the as-received AA2024 for tensile testing. The average values of the UTS and YS were plotted with error bars denoting the highest and lowest values. Figure 11 shows the variation of UTS and YS of the stir cast samples with yttrium addition. From Fig. 11, it can be observed that the UTS and YS of the samples follow the same trend as that of the hardness. There is a clear trend of increase in UTS and YS of the samples reinforced with yttrium compared to the as-received AA2024 sample. The UTS and YS increase up to 0.3 wt.% yttrium addition and tend to decrease upon a further increase in yttrium addition.

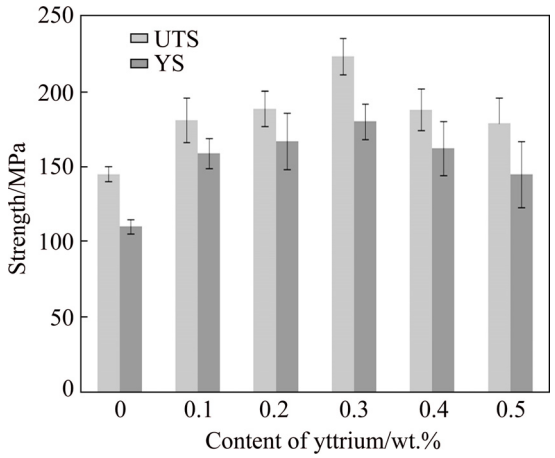

Fig. 11 Variation of UTS and YS of stir cast samples reinforced with varying amounts of yttrium addition

Figure 12 shows the variation of elongation of the samples reinforced with varying amounts of yttrium. From Fig. 12, an initial drop in elongation can be observed compared to the as-received AA2024 sample. Yttrium addition decreases the ductility of the samples. However, the elongation increases up to 0.3 wt.% yttrium addition and then tends to decrease. The elongation of the sample with 0.3 wt.% yttrium addition is observed to be higher than that of the as-received AA2024 sample.

Figure 13 shows the microstructures of the tensile fractured surfaces of the samples. As the yttrium content increases, deep dimples and cones are observed which are encircled in white and red colour. The samples undergo ductile fracture up to 0.3 wt.% yttrium addition, as observed from Figs. 13(a−d), in which there are a fair number of fine and deep dimples along with fine cones. As the yttrium addition increases beyond 0.3 wt.%, the dimples gradually increase in size with a decrease in depth and also intergranular fracture takes place, which leads to ductile−brittle fracture, as shown in Figs. 13(e, f).

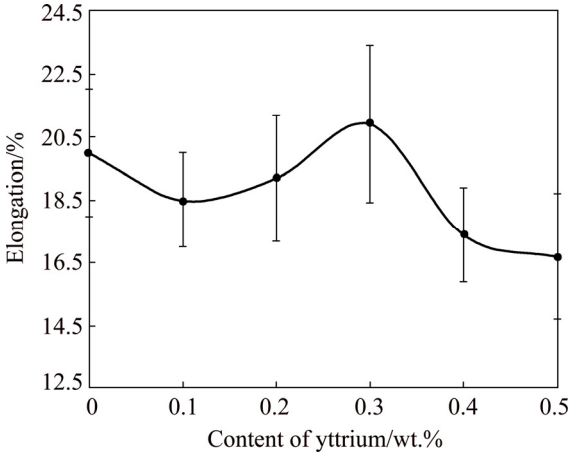

Fig. 12 Variation of elongation of stir cast samples with varying amounts of yttrium addition

4 Discussion

Addition of yttrium caused a steep drop in the density of the samples, as shown in Fig. 2. The drop in the relative density can be explained by the action of stirring during the multi-step stir casting process. During the process, when yttrium was introduced into the melt, micro air bubbles were formed as a result of stirring. Since no de-gassing was done in the present work, it was difficult for the air bubbles to escape naturally from the liquid melt either during stirring or solidification and also, the addition of yttrium hinders the release of air bubbles into the atmosphere. Hence, there was a decrease in the relative density of the samples as the yttrium addition increased. The air bubbles also affect the mechanical properties of the samples. However, the degradation in the mechanical properties caused by the air bubbles is very less as it can be observed that the densities of the samples are well above 99% and the difference between densities of the samples is less.

Through other studies, it was observed that the modification of microstructure by grain refinement was achieved by reinforcing a very little amount of rare earth elements that could effectively improve the overall mechanical properties of various aluminium alloys [13−31]. Addition of rare earth

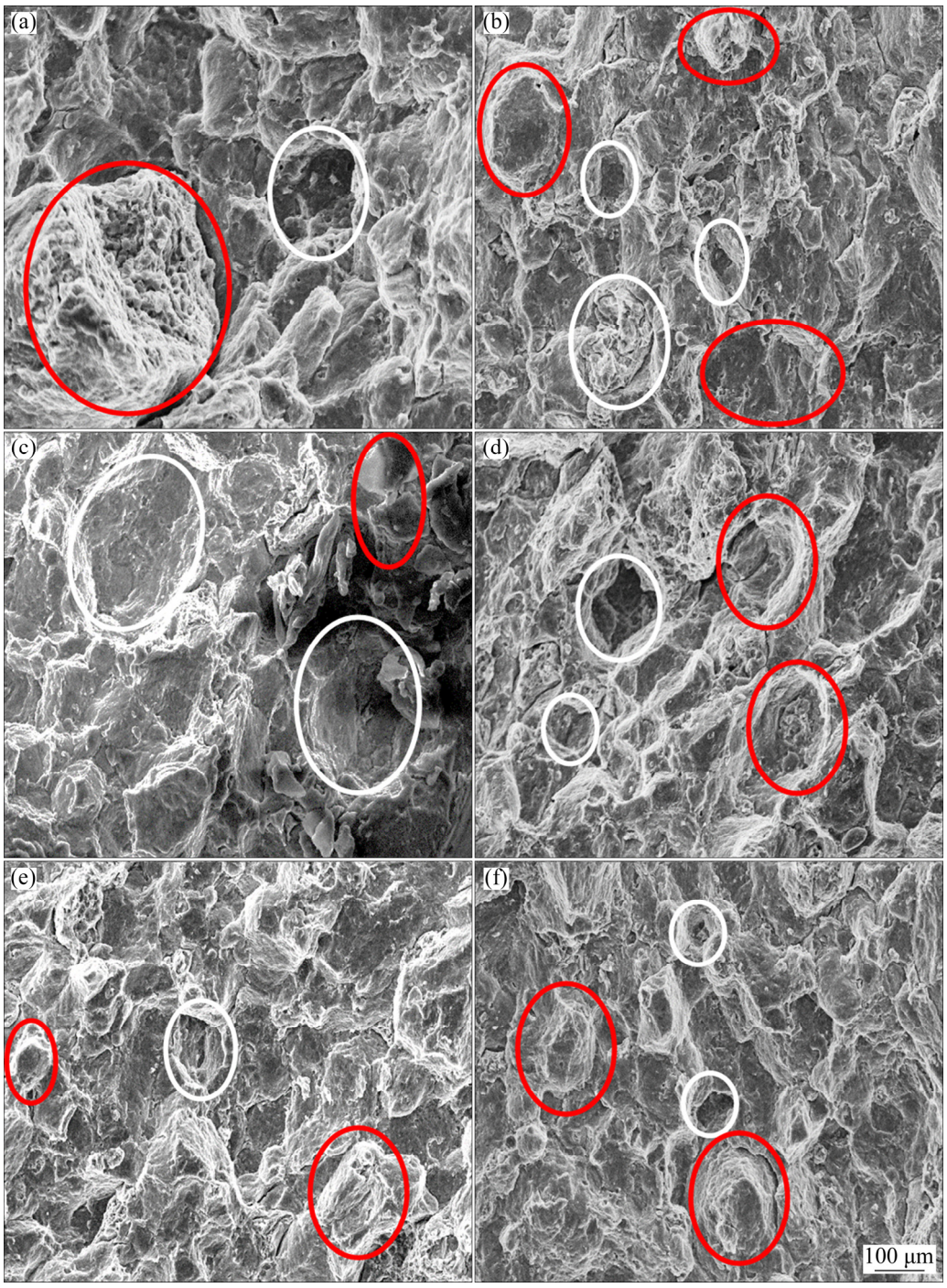

Fig. 13 SEM images of tensile fractured surfaces of samples with different amounts of yttrium addition: (a) 0 wt.%; (b) 0.1 wt.%; (c) 0.2 wt.%; (d) 0.3 wt.%; (e) 0.4 wt.%; (f) 0.5 wt.%

metal (yttrium) in very small amounts to the molten AA2024 sample brought significant changes in the microstructure by changing the morphology of the matrix metal from dendritic to spherical grains, as observed from Fig. 4. Yttrium addition is accompanied by grain modification and an increased tendency to form a non-dendritic grain structure. The effect of yttrium addition is manifested in the form of grain size modification, which affects the mechanical properties of the samples. The grain refinement in the matrix can be attributed to the difference in the atomic radius of aluminium and yttrium (r(Al)=0.143 nm and r(Y)=0.182 nm). The atomic radius of yttrium is bigger than that of aluminium and therefore, it is very difficult for yttrium atoms to enter into the

lattice of primary α(Al) phase. For this reason, yttrium concentrates in the front of the solid−liquid interface, restricting the growth of α(Al) grains and creating a strong constitutional under-cooling which leads to the nucleation of grains. The grain size of the samples initially decreases up to 0.3 wt.% yttrium addition and coarsens with further addition, as shown in Fig. 5.

A closer look at the microstructures at higher magnification, as shown in Fig. 7, revealed a secondary phase, which resembled a Chinese script shape. From the EDAX spectrum shown in Fig. 7(f) and the approximate elemental proportion given in Table 2, the Chinese script phase can be expected to be an Al−Cu−Y intermetallic [23,31]. From Fig. 3, it can be observed that the Chinese script intermetallic is Al_6Cu_6Y. As the yttrium addition increases, this Chinese script phase gets finer and also increases in amount up to 0.3 wt.%. Upon further increase in yttrium addition, the Chinese script phase coarsens. Another secondary phase was also observed in the microstructure having composition rich in Al and Cu. The EDAX spectrum of the phase is shown in Fig. 7(c) and its approximate elemental proportion detected by EDAX is given in Table 2. The secondary phases provide strength to the sample by obstructing the dislocation movement. Finer intermetallic and secondary phase present in the matrix can effectively resist the dislocation movement and hence modify the mechanical properties.

Mechanical properties of the samples like hardness, UTS, YS and elongation depend on the size and amount of the secondary phases present in the matrix and their ability to resist slipping and dislocation movement. The mechanical properties of the stir cast samples increase with an increase in the addition of yttrium. However, as the yttrium addition increases beyond 0.3 wt.%, the secondary phases become coarser and their effectiveness in resisting the dislocation decreases. Instead of offering dispersion strengthening, the coarse secondary phase, intermetallic phase, and precipitation start to behave like grains themselves and hence the mechanical properties deteriorate. This phenomenon could be due to the fact that the matrix alloy contains a variety of alloying elements like Cu, Mg, Mn and Fe. The elongation of the samples also follows the same trend as that of hardness, UTS and YS. However, an initial drop in the elongation is observed in the samples with the 0.1 wt.% addition of yttrium, as shown in Fig. 12. As the yttrium content increases, we can observe that the depth and number of the dimples increase. As the yttrium content increases beyond 0.3 wt.%, we can see that the dimples gradually disappear and intergranular fracture takes place, which leads to a near brittle fracture, as shown in Fig. 13.

CHEN et al [30] reported that when the amount of rare earth addition exceeds a certain value, the rare earth element will get segregated at the front of the solidification interface, as shown in Figs. 6(d, e) (encircled in red color) and prevent the diffusion of other alloying elements into the solid phase. This causes the solid solubility of alloying elements in the α(Al) matrix to decrease and hence increases the number of eutectic phases, causes segregation and reunion, hindering the refinement effect and make the entire organization begin to deteriorate.

2xxx series aluminium alloys are a class of heat treatable or age-hardenable alloys. AA2024 is very responsive to heat treatment. The widely used heat treatments to this alloy are T-3 (solution heat-treated (SHT), cold worked and naturally aged), T-4 (SHT and naturally aged) and T-6 (SHT and artificially aged). Natural aging requires a lot of time to get substantially stable condition and it follows an exponential trend. Hence, T-6 stands out to be a good alternative to T-3 and T-4 processes. The stir cast samples were heat-treated from 1 to 10 h at 190 °C. From Fig. 10, we can observe that the peak hardness was achieved in the samples heat-treated for 5 h irrespective of the amount of yttrium addition. Yttrium addition has accelerated the aging kinetics and brought down the peak age-hardening time to 5 h, compared to standard 10 h treatment. The phenomenon of acceleration of age hardening kinetics could be attributed to the increase in dislocation density due to thermal mismatch between the matrix and the reinforcing material. During quenching from solutionizing temperature, high density of dislocations along with excess vacancies are formed at the interface, which accelerates the kinetics of the diffusion process and causes the nucleation of precipitates [28,29].

Precipitates with an approximate composition of Al_2Cu were observed in the microstructures of peak hardened samples, as shown in Fig. 8(g) [30]. The precipitates become finer and increase in number as the yttrium addition increases and offer Orowan strengthening or precipitation strengthening to the samples. Beyond 0.3 wt.% yttrium addition, the precipitates coarsen, as shown in Fig. 8, and the strengthening effect decreases, leading to a drop in hardness. Before 5 h of heat treatment, the samples were in under-aged condition and after 5 h, they were in over-age condition.

5 Conclusions

(1) Addition of yttrium decreased the relative density of the samples.

(2) The microstructure analysis revealed that the addition of yttrium to α(Al) matrix refined the grains up to 0.3 wt.% by changing the morphology of secondary dendritic arm spacing (SDAS) and reducing the grain size. Beyond 0.3 wt.% yttrium addition, the grain refinement was not significant.

(3) Through EDAX analysis, two types of secondary phases rich in Al−Cu−Y and Al−Cu were identified in the matrix. The phase rich in Al−Cu−Y resembled a Chinese script shape and became finer and increased in amount as the yttrium addition increased to 0.3 wt.%. Upon further increase in yttrium addition, the script phase, as well as the Al−Cu phase coarsens. The main strengthening mechanisms in the samples were solid solution strengthening by Al−Cu phase, grain refinement and dispersion strengthening by Al−Cu−Y phase.

(4) Peak hardness of the heat-treated samples was achieved within 5 h. Yttrium addition reduced the heat treatment time to 5 h compared to the standard 10 h at 190 °C. Al_2Cu precipitation occurred due to heat treatment and the shape and size of the precipitates after at 5 h heat treatment depend on the variation of yttrium addition. The precipitation provided dispersion strengthening to the samples.

(5) The highest hardness of 66 HV was achieved for the sample with 0.3 wt.% yttrium addition and without any heat treatment. Similarly, the highest hardness of 90 HV was achieved for the same sample with heat treatment for 5 h. The hardness values achieved for the same sample with and without heat treatment were 146% and 200%, respectively, compared to the hardness of the as-received non-heat treated AA2024 sample.

(6) Highest UTS and YS achieved were 223 MPa and 180 MPa for the sample with 0.3 wt.% yttrium addition, 153% and 131% higher, respectively, compared to that of the as-received AA2024. The highest elongation achieved was 20.9%, which is 104% higher compared to that of the as-received AA2024 sample. However, the elongation decreased beyond 0.3 wt.% yttrium addition.

(7) From the results, it can be concluded that the optimum amount of yttrium addition to AA2024 matrix is 0.3 wt.%, which can create suitable conditions for the strengthening mechanisms to achieve the highest mechanical properties.

Acknowledgements

Authors would like to thank Indian Institute of Technology for providing experimental and characterization facilities.

References

[1] VOJTICH D. Challenges for research and development of new aluminium alloys [J]. Metalurgija, 2010, 49: 181−185. https://doi.org/10.1016/j.ymgme.2010.11.164.

[2] SURAPPA M K. Aluminium matrix composites: Challenges and opportunities [J]. Sadhana, 2003, 28: 319−334.

[3] SINCLAIR I, GREGSON P J. Structural performance of discontinuous metal matrix composites [J]. Materials Science and Technology, 1997, 13: 709−726. https://doi.org/10.1179/mst.1997.13.9.709.

[4] TOOZANDEHJANI M, KAMARUDIN N, DASHTIZADEH Z, LIM E Y, ASHEN G, CHANDIMA G. Conventional and advanced composites in aerospace industry: Technologies revisited [J]. American Journal of Aerospace Engineering, 2019, 5: 9−15. https://doi.org/10.11648/j.ajae.20180501.12.

[5] DASGUPTA R. The stretch, limit and path forward for particle reinforced metal matrix composites of 7075 Al-alloys [J]. Engineering, 2010, 2: 237−256. https://doi.org/10.4236/eng.2010.24034.

[6] CHRISTY TV, MURUGAN N, KUMAR S. A comparative study on the microstructures and mechanical properties of Al 6061 alloy and the MMC Al 6061/TiB_2/12p [J]. Journal of Minerals and Materials Characterization and Engineering, 2010, 9: 57−65. https://doi.org/10.4236/jmmce.2010.91005.

[7] AMIR J F, MEHRDAD A. 7xxx aluminum alloys; strengthening mechanisms and heat treatment: A review [J]. Material Science & Engineering International Journal, 2018,

2: 52−56. DOI: 10.15406/mseij.2018.02.00034.

[8] BUCHANAN K, COLAS K, RIBIS J, LOPEZ A, GARNIER J. Analysis of the metastable precipitates in peak-hardness aged Al−Mg−Si(−Cu) alloys with differing Si contents [J]. Acta Materialia, 2017, 132: 209−221. https://doi.org/10.1016/j.actamat.2017.04.037.

[9] FLAMENT C, RIBIS J, GARNIER J, SERRUYS Y, LEPRÊTRE F, GENTILS A, BAUMIER C, DESCOINS M, MANGELINCK D, LOPEZ A, COLAS K, BUCHANAN K, DONNADIEU P, DESCHAMPS A. Stability of β'' nano-phases in Al−Mg−Si(−Cu) alloy under high dose ion irradiation [J]. Acta Materialia, 2017, 128: 64−76. https://doi.org/10.1016/j.actamat.2017.01.044.

[10] CAMPBELL J. Sixty years of casting research [J]. Metallurgical and Materials Transactions A: Physical Metallurgy and Materials Science, 2015, 46: 4848−4853. https://doi.org/10.1007/s11661-015-2955-8.

[11] DASGUPTA R. Aluminium alloy-based metal matrix composites: A potential material for wear resistant applications [J]. ISRN Metallurgy, 2012, 2012: 1−14. https://doi.org/10.5402/2012/594573.

[12] ROJAS JI, NICOLAS J, CRESPO D. Study on mechanical relaxations of 7075 (Al−Zn−Mg) and 2024 (Al−Cu−Mg) alloys by application of the time-temperature superposition principle [J]. Advances in Materials Science and Engineering, 2017, 2017: 1−12. https://doi.org/10.1155/2017/2602953.

[13] SCOTT V D, KERRY S, TRUMPER R L. Nucleation and growth of precipitates in Al−Cu−Mg−Ag alloys [J]. Materials Science and Technology, 2013, 3: 827−835. https://doi.org/10.1179/mst.1987.3.10.827.

[14] ZOU Y, YAN H, YU B, HU Z. Effect of rare earth Yb on microstructure and corrosion resistance of ADC12 aluminum alloy [J]. Intermetallics, 2019, 110: 106−481. https://doi.org/10.1016/j.intermet.2019.106487.

[15] SHI Z, WANG Q, SHI Y, ZHAO G, ZHANG R. Microstructure and mechanical properties of Gd-modified A356 aluminum alloys [J]. Journal of Rare Earths, 2015, 33: 1004−1009. https://doi.org/10.1016/S1002-0721(14)60518-4.

[16] WANG H Y, LIU F, CHEN L, ZHA M, LIU G J, JIANG Q C. The effect of Sb addition on microstructures and tensile properties of extruded Al−20Mg2Si−4Cu alloy [J]. Material Science and Engineering A, 2016, 657: 331−338. https://doi.org/10.1016/j.msea.2016.01.063.

[17] LI Q, XIA T, LAN Y, LI P. Effects of rare earth Er addition on microstructure and mechanical properties of hypereutectic Al−20%Si alloy [J]. Materials Science and Engineering A, 2013, 588: 97−102. https://doi.org/10.1016/j.msea.2013.09.017.

[18] QIU H, YAN H, HU Z. Effect of samarium (Sm) addition on the microstructures and mechanical properties of Al−7Si−0.7Mg alloys [J]. Journal of Alloys and Compounds, 2013, 567: 77−81. https://doi.org/10.1016/j.jallcom.2013.03.050.

[19] DU J, DING D, ZHANG W, XU Zhou, GAO Yong-jin, CHEN Guo-zhen, YOU Xiao-hua, CHEN Ren-zong, HUANG Yuan-wei, TANG Jin-song. Effect of Ce addition on the microstructure and properties of Al−Cu−Mn−Mg−Fe lithium battery shell alloy [J]. Material Characterization, 2018, 142: 252−260. https://doi.org/10.1016/j.matchar.2018.05.049.

[20] MAO F, YAN G, XUAN Z, CAO Z, WANG T. Effect of Eu addition on the microstructures and mechanical properties of A356 aluminum alloys [J]. Journal of Alloys and Compounds, 2015, 650: 896−906. https://doi.org/10.1016/j.jallcom. 2015.06.266.

[21] WU X F, WANG K Y, WU F F, ZHAO R D. Simultaneous grain refinement and eutectic Mg_2Si modification in hypoeutectic Al−11Mg_2Si alloys by Sc addition [J]. Journal of Alloys and Compounds, 2019, 791: 402−410. https://doi.org/10.1016/j.jallcom.2019.03.326.

[22] TANG Q, ZHAO J, WANG T, CHEN J, HE K. The effects of neodymium addition on the intermetallic microstructure and mechanical properties of Al−7Si−0.3Mg−0.3Fe alloys [J]. Journal of Alloys and Compounds, 2018, 741: 161−173. https://doi.org/10.1016/j.jallcom.2018.01.138.

[23] LI Q, LI B, LI J, ZHU Y, XIA T. Effect of yttrium addition on the microstructures and mechanical properties of hypereutectic Al−20Si alloy [J]. Materials Science and Engineering A, 2018, 722: 47−57. https://doi.org/10.1016/j.msea.2018.03.015.

[24] MEDVEDEV A, MURASHKIN M Y, ENIKEEV N, VALIEV R Z, HODGSON P D, LAPOVOK R. Enhancement of mechanical and electrical properties of Al−RE alloys by optimizing rare-earth concentration and thermo-mechanical treatment [J]. Journal of Alloys and Compounds, 2018, 745: 696−704. https://doi.org/10.1016/j. jallcom.2018.02.247.

[25] SONG X, YAN H, ZHANG X. Microstructure and mechanical properties of Al−7Si−0.7Mg alloy formed with an addition of (Pr+Ce) [J]. Journal of Rare Earths, 2017, 35: 412−418. https://doi.org/10.1016/S1002-0721(17)60927-X.

[26] YAN H, CHEN F, LI Z. Microstructure and mechanical properties of AlSi10Cu3 alloy with (La+Yb) addition processed by heat treatment [J]. Journal of Rare Earths, 2016, 34: 938−944. https://doi.org/10.1016/S1002-0721(16)60118-7.

[27] ZHANG X M, WANG W T, CHEN M A, GAO Zhi-guo, JIA Yu-zhen, YE Ling-ying, ZHENG Da-wei, LIU Ling, KUANG Xiao-yue. Effects of Yb addition on microstructures and mechanical properties of 2519A aluminum alloy plate [J]. Transactions of Nonferrous Metals Society of China, 2010, 20: 727−731. https://doi.org/10.1016/ S1003-6326(09)60205-3.

[28] REN X, PENG L, HUANG G, ZONG R, XIE H, LI J. Effect of Nd on microstructure and properties of 2A70 alloy [J]. Journal of Alloys and Compounds, 2018, 731: 1014−1021. https://doi.org/10.1016/j.jallcom.2017.10.136.

[29] BAI S, YI X, LIU G, LIU Z, WANG J, ZHAO J. Effect of Sc addition on the microstructures and age-hardening behavior of an Al−Cu−Mg−Ag alloy [J]. Materials Science and Engineering A, 2019, 756: 258−267. https://doi.org/10.1016/j.msea.2019.04.045.

[30] CHEN X, LIU Z, BAI S, LI Y, LIN L. Alloying behavior of erbium in an Al−Cu−Mg alloy [J]. Journal of Alloys and Compounds, 2010, 505: 201−205. https://doi.org/10.1016/j.jallcom.2010.06.029.

[31] LI H Z, LING X P, LI F F, GUO F F, LI Z, ZHANG X M. Effect of Y on microstructure and mechanical properties of 2519 aluminium alloy [J]. Transactions of Nonferrous Metals Society of China, 2007, 17(6): 1191−1198.

添加钇和时效对多级搅拌铸造 AA2024 力学性能的影响

CH. S. VIDYASAGAR[1], D. B. KARUNAKAR[2]

1. Metallurgical and Materials Engineering Department, Indian Institute of Technology Roorkee - 247667, India;
2. Mechanical and Industrial Engineering Department, Indian Institute of Technology Roorkee - 247667, India

摘　要：研究钇和人工时效对 AA2024 的影响。样品在 190 °C 人工时效 1~10 h，时效时间间隔为 1 h。采用扫描电子显微镜和 X 射线衍射对样品进行表征，利用维氏硬度试验机和万能试验机对样品进行硬度和拉伸强度等力学性能测试。显微组织显示，添加钇能够细化 α(Al)基体，并形成汉字形状的 Al−Cu−Y 金属间化合物强化相。与母材相比，添加钇的试样具有更好的力学性能。添加 0.3%钇(质量分数)的样品表现出最高的力学性能，其硬度为 66 HV、极限抗拉强度(UTS)为 223 MPa、屈服强度(YS)为 180 MPa、伸长率为 20.9%。人工时效样品表明，在 190 °C 时效 5 h 内，所有样品均出现峰值硬化，且均有 Al_2Cu 析出。随着时效的延长，汉字形状的金属间化合物逐渐演变为纤维状。AA2024 中钇的最佳添加量为 0.3%(质量分数)。

关键词：钇；人工时效；力学性能；多级搅拌铸造；析出；显微组织表征

(Edited by Bing YANG)